JOURNAL OF PROPULSION AND POWER
Vol. 15, No. 3, May–June 1999

Design of Three-Dimensional Hypersonic Inlets with Rectangular-to-Elliptical Shape Transition

M. K. Smart*
NASA Langley Research Center, Hampton, Virginia 23681

A methodology has been devised for the design of three-dimensional hypersonic inlets. This methodology makes extensive use of inviscid stream-tracing techniques to generate an inlet with smooth shape transition from a rectangular-like capture to an elliptical throat. Highly swept leading edges and a significantly notched cowl enable use of these inlets in fixed geometry configurations. The design procedure includes a three-dimensional viscous correction and uses established correlations to check for boundary-layer separation caused by shock-wave interactions. Complete details of the design procedure are presented and the characteristics of a modular inlet with a design point of Mach 6.0 are examined. Comparison with a classical two-dimensional inlet optimized for maximum total pressure recovery indicates that these three-dimensional inlets demonstrate good inviscid performance even when operating well below the design point. An estimate of the on-design viscous performance corresponds with that of an efficient inlet for scramjet applications.

Nomenclature

A	= area
C_D	= drag coefficient, $D_{\text{inv}}/0.5\gamma P_1 M_1^2 A_{\text{aero}}$
C_f	= skin friction coefficient
CRI	= internal contraction ratio of inlet
CRT	= total contraction ratio of inlet
D_{inv}	= inviscid drag
d_h	= hydraulic diameter of the inlet throat
H	= two-dimensional inlet throat height
h_1, h_2	= metrics of the x and z coordinates
L	= length
M	= Mach number
m_c	= mass capture percentage
P	= pressure
P_R	= inlet compression ratio, P_{ex}/P_1
P_T	= total pressure recovery, $(P_t)_{\text{ex}}/(P_t)_1$
P_t	= total pressure
q	= dynamic pressure
Re	= Reynolds number
R_0	= radius of axisymmetric compression field capture
r	= radius
s	= distance along streamlines
T	= temperature
T_R	= inlet temperature ratio, T_{ex}/T_1
u, v, w	= velocity components
W	= two-dimensional inlet width
x, y, z	= coordinate directions
α	= parameter in lofting procedure
β	= boundary-layer crossflow angle
γ	= ratio of specific heats
δ	= boundary-layer thickness
δ^*	= boundary-layer displacement thickness
η_{KD}	= process efficiency
η_{KE}	= kinetic energy efficiency
θ	= flow turning

Subscripts

aero	= aerodynamic capture
ca	= inlet capture
cc	= cowl closure
e	= boundary-layer edge
ex	= inlet exit conditions, $x/R_0 = 8.0$
i	= incipient separation
inl	= inlet
is	= isolator
mfw	= mass flow weighted
N	= component normal to the shock
vis	= viscous
w	= wetted surface
1	= inlet entrance conditions

Introduction

THE design of efficient inlets for hypersonic vehicles utilizing airframe-integrated scramjet modules is a subject of interest at NASA Langley Research Center. In these configurations, the vehicle bow shock performs the initial compression, and the capture shape for the inlet of each scramjet module is required to form three sides of a rectangle so that the modules may be mounted side-by-side. Other requirements are that the inlets have good starting characteristics at ramjet takeover speeds (Mach 3–4) and operate efficiently up to the vehicle cruise condition. To reduce structural complexity, there is also a strong preference for an inlet with fixed geometry and no requirement for boundary-layer bleed. A further desirable inlet feature for some scramjet applications is a cross-sectional shape transition to an elliptical throat. The inlet may then be used in combination with an elliptical combustor, which is superior to a rectangular cross section in terms of the structural weight required to contain a specified pressure and the wetted surface area needed to enclose a specified flow area. Fluid dynamic problems associated with hypersonic corner flows are also minimized with this type of configuration. The aforementioned inlet features constitute a set of stringent requirements, some of which will not be able to be met in a practical vehicle. Hypersonic inlets designed using fully three-dimensional design methodologies may be able to satisfy many of these demands.

A number of three-dimensionally curved hypersonic missile inlets with circular or elliptical throats were designed and tested in the 1960s by Hartill,[1] Kiersey and Snow,[2] and Kutshenreuter.[3] These fixed geometry inlets showed good performance in the wind tunnel and self-started at internal contraction ratios well above the one-dimensional inviscid starting limit determined by Kantrowitz and

Presented as Paper 98-0960 at the AIAA 36th Aerospace Sciences Meeting, Reno, NV, Jan. 6–9, 1997; received March 8, 1998; revision received July 18, 1998; accepted for publication July 30, 1998.

*Research Associate, National Research Council, Hypersonic Airbreathing Propulsion Branch, M/S 168. Senior Member AIAA.

Donaldson.[4] However, the performance of this inlet class was difficult to predict with the computational tools available at that time. In the mid-1980s, Simmons and Wiedner[5] produced a thorough literature review of three-dimensional hypersonic inlet design and described a conceptual design methodology for inlets with rectangular capture and circular throat. This methodology was an adaption of the 1960's design procedures to modular scramjet configurations, and comprised a stream-tracing technique used in combination with a lofting procedure for cross-sectional shape transition. Unfortunately, no detailed design and testing of inlet configurations was performed as a result of this study. An interesting article by Billig[6] described the design and wind-tunnel testing of a scramjet missile concept between 1962 and 1978. This missile included a three-dimensionally curved inlet based on tracing streamlines through an internal conical compression flowfield as described in Ref. 2.

The aim of the current project is the development of a complete design methodology for three-dimensional hypersonic inlets. This project has been undertaken to examine the possible advantages of three-dimensional inlet geometries relative to more traditional inlets based on two-dimensional design methodologies. Extensive use of three-dimensional computational tools is essential for this work, and the methodology utilizes many of the ideas developed in the aforementioned inlet studies.[1–3,5] Preliminary work on this project, presented in Ref. 7, involved the design of stream-traced hypersonic inlets. The current article extends this work to hypersonic inlets in which the shape of the inlet capture and throat are specified a priori, something not able to be accomplished using stream-tracing techniques alone. In particular, the work concentrates on inlets with rectangular-to-elliptical shape transition (REST). The constraints placed on the inlets designed in this work are suitability for modular scramjet applications, fixed geometry, no boundary-layer bleed, and no large boundary-layer separations. Given the self-starting capabilities exhibited by the inlets described in Refs. 1–3, internal contraction ratios are kept as low as possible, but are not required to satisfy the Kantrowitz limit. Complete details of the design methodology are presented and the characteristics of a REST inlet with a design point of Mach 6.0 are examined.

REST Inlet Design Methodology

General Remarks

While computational methods and computer speed have improved markedly during the past 10 years, full Navier–Stokes calculations of turbulent three-dimensional hypersonic inlet flows are not yet a practical design tool. In the current work, the inlet design methodology utilizes three-dimensional inviscid calculations to determine the shock structure and surface pressure signature of inlet shapes. This information is then compared with empirical correlations to check for boundary-layer separations resulting from shock-wave interactions. A three-dimensional boundary-layer calculation is then performed to determine the physical inlet shape that generates the inviscid flowfield. With the use of current supercomputers and computational fluid dynamics (CFD) codes, the cycle time for this process can be reduced to the point where numerous design iterations can be performed in a few working days.

A complete inlet design procedure is logically separated into two sections: 1) determination of the inviscid inlet shape, and 2) calculation of the viscous correction. The inviscid portion of the design procedure is summarized in this section. A description of the technique used to calculate the three-dimensional viscous correction to the inviscid shape is presented later. While the inviscid inlet shapes generated using this methodology do not coincide with the streamlines through any known flowfield; i.e., they cannot be called *stream-traced inlets*, a modified stream-tracing technique forms the basis of the inviscid portion of the design procedure. This will first be summarized, followed by a description of how stream-traced shapes may be combined to construct an inlet with a specified shape transition. The inviscid portion of the design procedure is completed by a brief description of the use of established shock-wave/boundary-layer separation criteria for the types of turbulent shock interactions that occur in REST inlets.

Stream-Traced Inlets

The stream-tracing process provides a powerful but relatively simple technique for determining the inviscid shape of an inlet with a predetermined capture shape and pressure ratio. The general steps are as follows.

1) Construct a desirable compressive flowfield that has the same entrance Mach number and pressure ratio as required for the inlet. In practice, this flowfield is usually chosen to be either two dimensional or axisymmetric.

2) Define a capture shape that fits within the entrance of the compression field.

3) Calculate the path of the streamlines that pass through the perimeter of the capture shape. The stream surface defined by these streamlines constitutes the inviscid shape of the inlet.

The key to the design of efficient stream-traced inlets is the choice of the compression field through which the streamlines are traced. Whatever features are contained in this flowfield will also be a part of the flowfield generated inside the inlet. The current choice for the form of this flow is an axisymmetric compression field with a constant radius centerbody. This flowfield, a schematic of which is shown in Fig. 1, takes advantage of the isentropic compression inherent in axisymmetric compression fields, whereas the centerbody removes the flow region near the axis where shock focusing can lead to high losses. The outer surface shape is determined by a tradeoff between maximum total pressure recovery, maximum shock strength that will not produce boundary-layer separation, minimum length, and minimum exit flow nonuniformity. In the current work, a preliminary shape is determined by reversing an axisymmetric expansion nozzle profile with centerbody radius, throat Mach number, and pressure ratio similar to the desired inlet. The profile is then shortened by converting the initial portion to a finite lip angle. Finally, some iteration of the centerbody radius and throat shape is performed so that significant canceling of the axisymmetric shock wave occurs at the throat. This process has been found to generate axisymmetric compression fields suitable for practical inlet configurations.

Once the compression field has been calculated, a multitude of possible capture shapes are available to the inlet designer. The modular application of the current work requires that the capture shape have parallel sides and a straight top at right angles to the sides; however, the bottom (or cowl) can be of a more general shape. Typically, the largest desired capture shape that fits within the annular entrance flow is chosen to minimize the inlet length/cross-sectional area ratio. Figure 1 shows the inlet formed by a rectangular capture shape. Note that streamlines passing through the capture perimeter remain straight, up to the point each encounters the shock surface, allowing the side leading edges of the inlet to be highly swept and the cowl to be notched. It is this characteristic of the current design methodology that enables the inlet to operate well below its design point by spilling flow below the cowl.

In the current work, the axisymmetric compression fields were calculated using the NASA Langley Research Center's program, SEAGULL, which is an inviscid shock-fitting code specifically

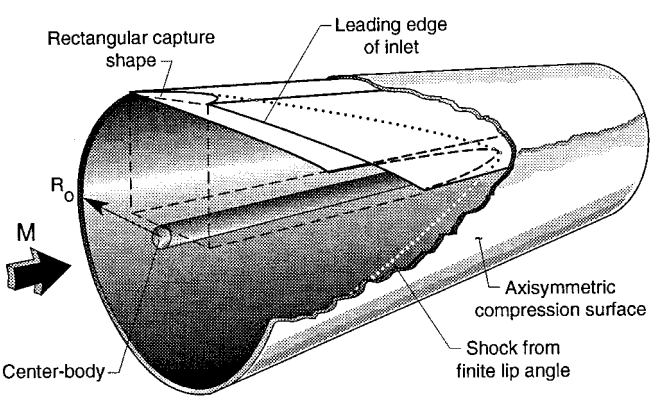

Fig. 1 Schematic of a stream-traced inlet based on an axisymmetric compression field.

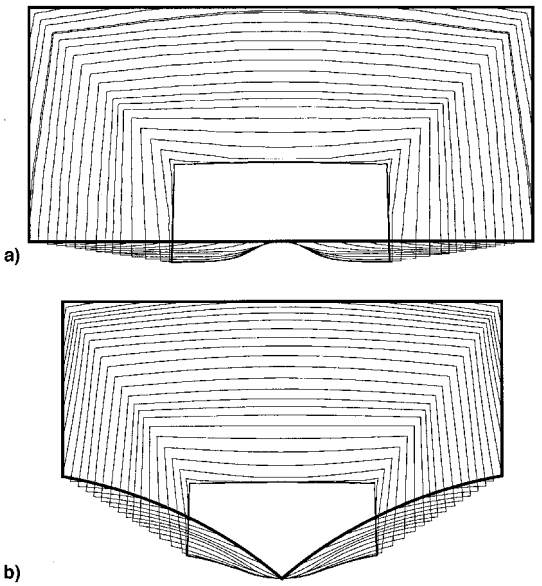

Fig. 2 Inlet cross-sectional shape distributions for different capture perimeters: a) Rectangular capture shape and b) capture shape used for REST inlets.

designed for supersonic internal flows.[8] Once the axisymmetric compression field is calculated, the paths of streamlines passing through the capture shape are determined using the stream-tracing routine in the plotting program TECPLOT.[9] Figure 2a shows the distortion of a rectangular capture shape as the streamlines pass through a typical axisymmetric compression field. Note that this capture shape leads to a convex bump on the cowl surface that is not acceptable for a practical inlet. A capture shape that generates a more suitable cross-sectional distribution throughout the compression field is shown in Fig. 2b. This capture shape still satisfies the modular requirements of the current work, but the curved bottom edge of the capture shape leads to a more desirable cross-sectional shape at the inlet throat. The inlet represented in Fig. 2b typifies the stream-traced shape that is adapted in the current work to allow independent specification of both capture and throat shapes.

Inlet Shape Transition

Streamline tracing techniques enable the generation of an inlet shape that has characteristics almost identical to a predetermined flowfield, but an independently specified capture shape. Similarly, stream-tracing techniques enable the determination of an inlet shape with characteristics nearly identical to a predetermined flowfield, but with an independently specified throat shape. This can be obtained by simply tracing streamlines backward through the flowfield. In the current methodology, an inlet with an independently specified capture and throat is determined by combining a number of stream-traced shapes to produce a smooth transition from capture to throat. If this combination of stream-traced shapes is done in a judicious way, the resultant inlet shape can produce an inviscid flowfield with characteristics only slightly degraded from the original flowfield.

Of particular interest in the current work is the generation of inlets with transition from a rectangular-like capture shape to an elliptical throat (REST). The steps used to perform this are as follows.

1) Calculate a desirable axisymmetric compression field that has the same entrance Mach number and pressure ratio as required for the inlet.

2) Generate a stream-traced inlet shape using a rectangular-like capture shape such as that shown in Fig. 2b; this is designated as shape A.

3) Generate a second stream-traced inlet shape using a capture shape similar to shape A, but with radiused corners; this is designated as shape B.

4) Generate a third inlet shape that has an elliptical throat of the same area as shape A; this is designated as shape C.

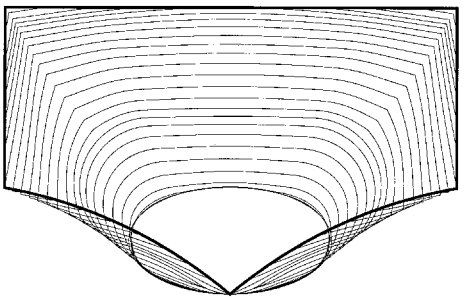

Fig. 3 Cross-sectional shape distribution for a REST inlet.

5) Smoothly combine all three inlet shapes to form a REST inlet that has the capture shape of A, the cross-sectional shape of B at cowl closure, and the same throat shape as C.

Smooth shape transition between the three stream-traced inlets is accomplished in the current work with a mathematical lofting procedure developed by Barger.[10] This procedure enables smooth transition from an initial to a final shape with a remaining free parameter that can be adjusted, in this instance, to optimize the REST inlet for maximum total pressure recovery or minimum exit flow nonuniformity. For example, if $f_1(y)$ and $f_2(y)$ represent the cross sections of shapes A and B at some intermediate station between inlet capture (x_{ca}) and cowl closure (x_{cc}), then the cross section of the REST inlet at the intermediate station is given by

$$f(y) = [f_1(y)]^{1-E(x)}[f_2(y)]^{E(x)} \tag{1}$$

where

$$E(x) = \left(\frac{x - x_{ca}}{x_{cc} - x_{ca}}\right)^{\alpha}, \qquad \alpha > 0$$

Combining cross sections in this way smooths out regions of high curvature. Values of α ranging between 1.0 and 5.0 have been found to supply sensible shape transitions for the current application. Figure 3 shows a typical cross-sectional shape distribution for a REST inlet with $\alpha = 3.5$. Once the coordinates of the REST inlet cross-sectional shapes are known, they are used to generate a computational grid for calculating the flowfield generated by the inlet. It is noted that while the on-design performance of a stream-traced inlet is already predetermined as part of the design procedure, the determination of both the on and off-design performance of the REST inlet requires the use of fully three-dimensional computational methods.

Shock-Wave/Boundary-Layer Interactions

It is of considerable importance to include some treatment of turbulent shock-wave/boundary-layer interactions in the inviscid portion of the inlet design procedure. Shock-induced boundary-layer separation can produce significant losses within the inlet, and may cause inlet unstart. Large separated regions also invalidate the use of the boundary-layer equations for calculating the viscous correction needed to determine the physical shape of the inlet. Established incipient separation criteria for turbulent interactions are employed in the current work to determine the maximum shock strength allowable within the inlet. In practice, it is the desire to inhibit boundary-layer separation that sets a limit on the minimum length of an inlet.

Shock-wave/boundary-layer interactions are generally separated into two categories:

1) Two-dimensional interactions such as those that occur at an unswept compression ramp or when a planar oblique shock reflects at a surface.

2) Swept interactions, such as the interaction produced by a planar oblique shock wave as it sweeps across a flat plate from a perpendicular fin.

Incipient separation criterion for turbulent boundary layers have been established for both these types of interactions, most notably by Korkegi.[11] For two-dimensional interactions, the pressure

rise for incipient separation increases rapidly with Mach number. Conversely, incipient separation of swept interactions is independent of freestream Mach number and occurs at a pressure ratio of $P_i/P \approx 1.5$; i.e., when the Mach number component normal to the shock reaches $M_N \approx 1.2$. The shock-wave/boundary-layer interactions that occur in the inlets designed using the current methodology do not belong to either category. These involve the reflection of curved shocks at smoothly curved surfaces, where the line of reflection is generally swept back with respect to the oncoming flow. In a typical REST inlet, the incident shock reflects at the crotch of the cowl, sweeps across the bottom and side surfaces, and strikes the top surface at the throat. For these *mixed* interactions, Korkegi[12] suggested that M_N is the most dominant parameter for determining incipient separation. Given this, the two-dimensional incipient separation criterion of Ref. 11 is applied to the mixed interactions of interest in the current work as follows:

$$P_i/P = 1.0 + 0.3M_N^2, \qquad M_N < 4.5 \tag{2a}$$

$$P_i/P = 0.17M_N^{2.5}, \qquad M_N \geq 4.5 \tag{2b}$$

If the sweep angle of a mixed interaction is defined as the angle between the line perpendicular to the flow and the line parallel with the shock wave, this criterion can be plotted as shown in Fig. 4. Note that at a given Mach number, the pressure rise for incipient separation of a mixed interaction lies between a maximum defined by the two-dimensional interaction (sweep angle = 0.0 deg) and a minimum associated with the swept interaction. Equation (2) is utilized in this manner for the REST inlet design test case described in the next section.

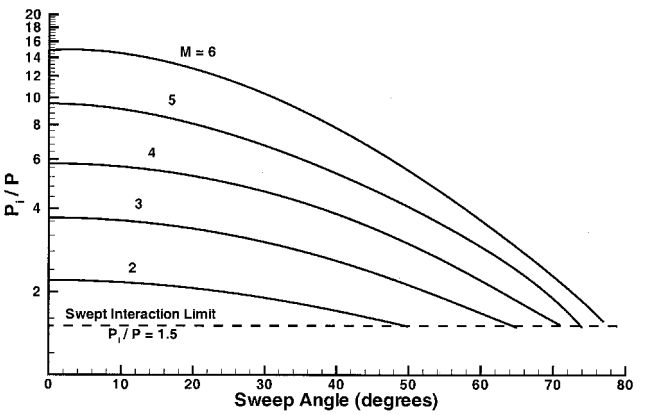

Fig. 4 Incipient separation limits for mixed shock-wave/boundary-layer interactions.

Inviscid Performance of a Mach 6.0 REST Inlet

Shape Determination

The design methodology described in the previous section is applied in the current paper to a scramjet inlet module mounted beneath a vehicle cruising at $M = 7.1$. The vehicle is assumed to travel on a constant $q = 50$-kPa trajectory. In combination with a 6-deg forebody compression, the inlet is required to supply the scramjet combustor with flow at $P = 50$ kPa. Flow enters the inlet at $M_1 = 6.0$ in this instance, and the required inlet compression ratio is $P_R = 13.50$. All calculations performed for this paper assume airflow at $\gamma = 1.4$.

Pressure contours in the axisymmetric compression field calculated for this case are shown in Fig. 5 (with the vertical scale magnified to aid visualization). In this instance, a lip angle of 4 deg and a centerbody radius of $r/R_0 = 0.10$ were used. These values result from a compromise between minimum length and the requirement for no boundary-layer separation. The throat profile and its position were chosen to perform the maximum amount of shock cancellation, leading to a relatively uniform exit flow. The characteristics of a REST inlet constructed using this flowfield will depend on how the different stream-traced shapes are combined to form the required shape transition. After iteration involving the geometry of the bottom edge of the capture shape, the radii of the corners at cowl closure, the aspect ratio of the throat, and the α used in the lofting procedure, the REST inlet shown in Fig. 6 was generated. This iteration required the use of the fully three-dimensional computational methods described in the next subsection. Note the significant sweep of the side leading edges of the inlet, the extensive notch in the cowl, and the transition from a capture shape with pronounced corners to a throat with elliptical cross section. The overall contraction ratio for this inlet is $CRT_{inv} = 5.92$. Internal contraction begins in these inlets at cowl closure. Based on the cross-sectional area perpendicular to the entrance flow at cowl closure, the internal contraction ratio of the inlet is $CRI_{inv} = 2.34$.

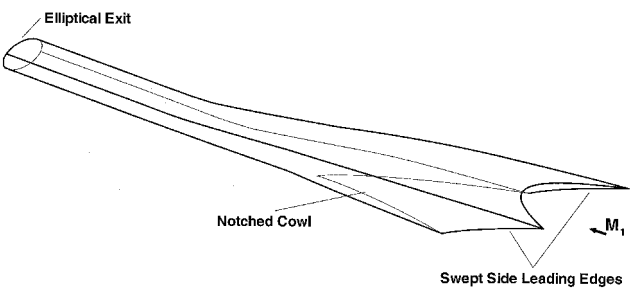

Fig. 6 Pictorial view of the Mach 6.0 REST inlet.

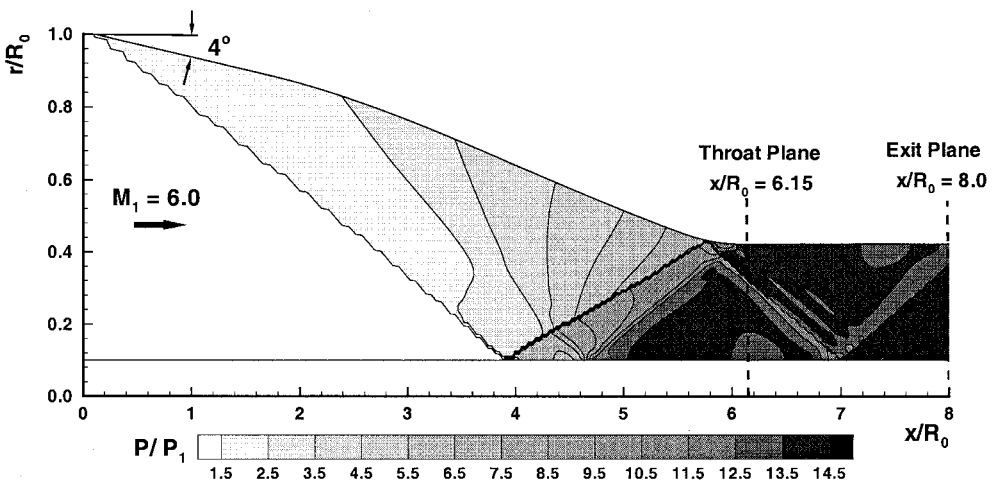

Fig. 5 Axisymmetric compression field used to design the Mach 6.0 REST inlet.

Three-Dimensional Inviscid Flow Calculations

The three-dimensional inviscid flowfields generated by the inlet shown in Fig. 6 have been calculated using the CFD code GASPv3 (Ref. 13). This code utilizes cell-centered, finite volume, upwind methods to solve the three dimensional, unsteady, compressible Euler equations. A mixed topology grid was found to be the most suitable for REST inlet calculations. This grid consisted of 545 planes normal to the freestream direction with each plane containing a central 37×37 H-type mesh constructed within a peripheral 17×109 C-type mesh as depicted in Fig. 7. This type of grid allowed for a smooth transition from the cornered entrance plane to the elliptical exit without unsatisfactory cell distortion. Typical CPU times of 14 min were obtained on a Cray C-90 for space-marching calculations with four orders of magnitude convergence. A 50% increase in the number of grid points in both cross-plane directions showed little change in the flowfield solution. For the present calculations, the inlet is assumed to be mounted underneath the vehicle and between identical modules. Flow spillage upstream of the notched cowl is modeled by using an extrapolation boundary condition for boundary cell faces ahead of the leading edge.

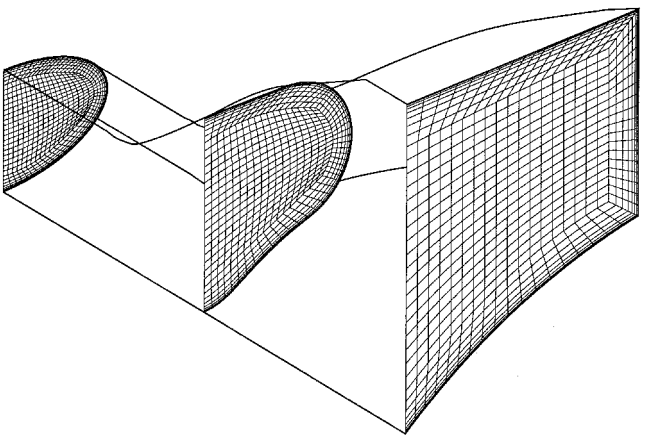

Fig. 7 Schematic showing three planes in a typical computational grid.

Inviscid flowfield calculations have been performed at the $M_1 = 6.0$ design condition as well as at $M_1 = 4.8$ and 3.6. A comparison of the results of these calculations provides insight into the development of the inlet flow structure as the vehicle accelerates to cruise conditions. Figures 8a–8c show pressure contours in the symmetry plane of the inlet at $M_1 = 3.6$, 4.8, and 6.0, respectively (with the vertical scale magnified to aid visualization). At Mach 3.6, the inlet shows considerable spillage below the notched cowl, and the cowl shock strikes the top surface well upstream of the throat. Minimal shock cancellation occurs in this instance, and an extensive shock system can be seen downstream of the throat. At Mach 4.8, the shock waves in the flow are swept farther downstream, leading to considerably less spillage than at Mach 3.6. Some shock cancellation does occur at the inlet throat; however, significant flow nonuniformity persists at the inlet exit ($x/R_0 = 8.0$). At the Mach 6.0 design point, the leading shock wave passes only slightly upstream of the cowl and the cowl shock is almost canceled at the throat ($x/R_0 = 6.15$). Minimal spillage occurs in this instance and the flow structure, while not being identical to the original axisymmetric compression field, is only slightly degraded in terms of exit flow nonuniformity and total pressure recovery. Given the significant shape transition of the inlet, reduction of flow degradation relative to the original compression field to the level observed here is considered to be a significant achievement.

Figure 9 shows a pictorial view of the REST inlet with surface pressure contours corresponding to the $M_1 = 6.0$ inviscid flowfield. Note that the top surface pressure distribution contains very little lateral variation upstream of the throat, indicating that it does not see any swept shock waves. Swept shock-wave/boundary-layer interactions involving the top surface boundary layer (which has generally been ingested from the forebody), are a considerable problem for side-wall compression inlets. In the current configuration, only the side and bottom inlet surfaces encounter swept shock waves. These interactions have a less significant effect on the overall performance of the inlet, as the boundary-layer thickness is considerably less than on the top surface. Checks for boundary-layer separation have

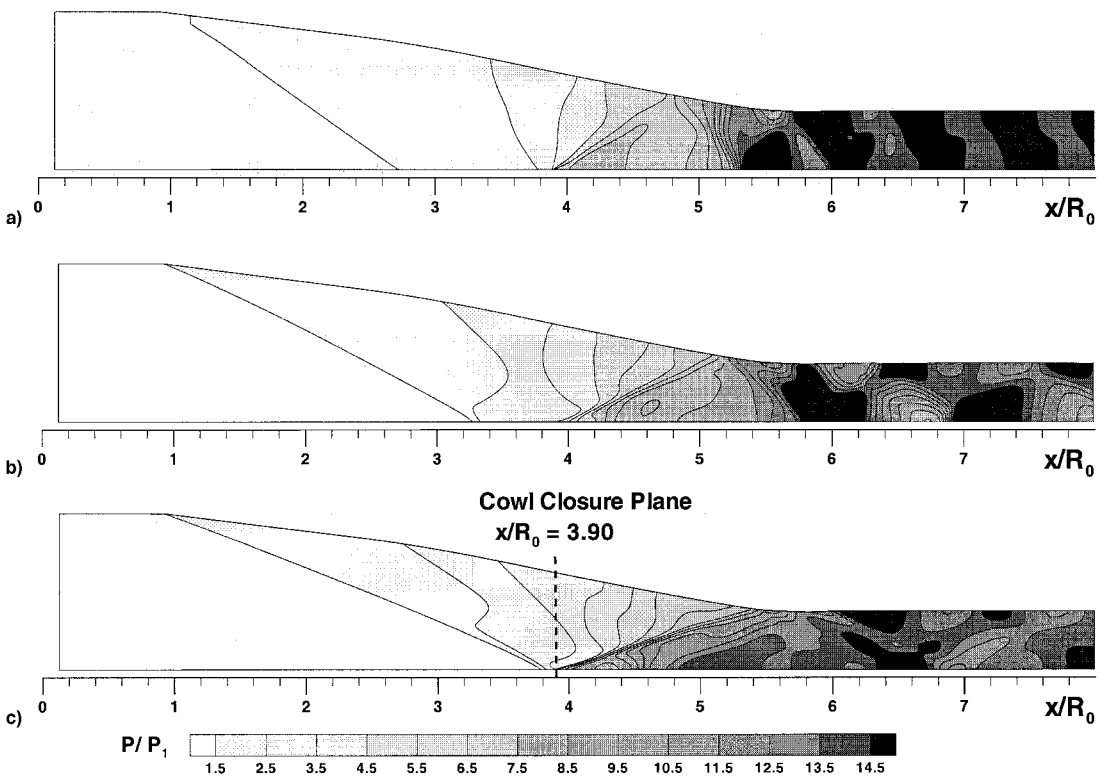

Fig. 8 Symmetry plane pressure contours generated by the Mach 6.0 REST inlet at different Mach numbers. M = a) 3.6, b) 4.8, and c) 6.0.

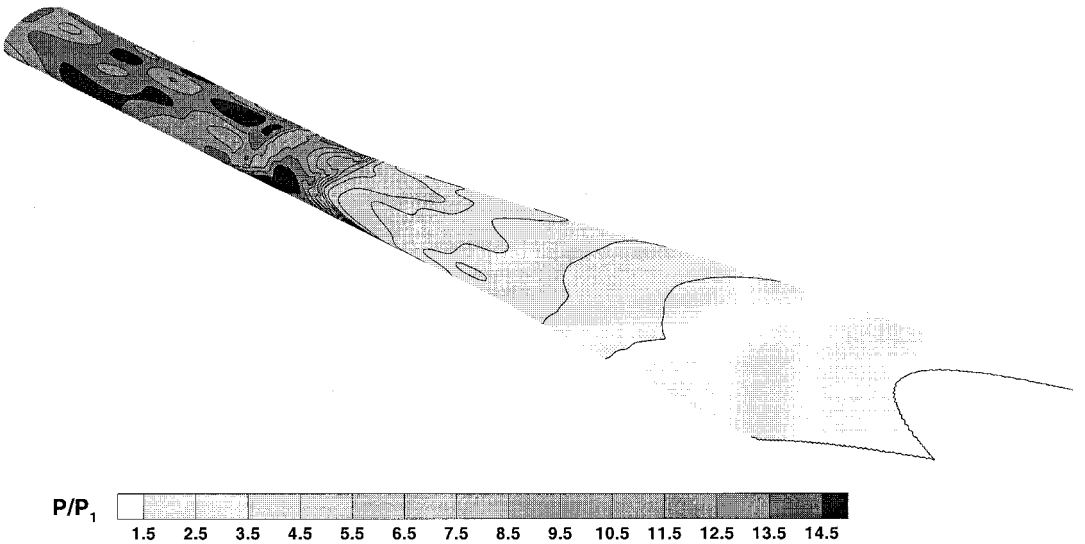

Fig. 9 Pictorial view showing surface pressure contours in the on-design Mach 6.0 REST inlet flowfield.

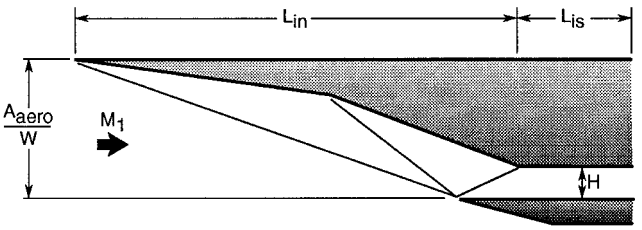

Fig. 10 Schematic of the two-dimensional inlet used for performance comparison.

been made for the turbulent shock-wave/boundary-layer interactions associated with this flowfield, using the procedure outlined in the previous section. These indicated that the swept interaction on the bottom surface may induce some level of separation, while interactions on the top and side surfaces are below the incipient separation limit. A swept separation of the thin bottom surface boundary layer is not considered to have a significant effect on practical inlet operation in this instance.

Table 1 lists some properties of the inlet flowfield at the exit plane ($x/R_0 = 8.0$), including mass capture percentage, compression ratio, temperature ratio, and exit Mach number. These properties were calculated by converting the nonuniform exit flowfield to an equivalent one-dimensional flow with the same total enthalpy, axial stream thrust, cross-sectional area, and mass flow. The listed property variations correspond to the percentage property range about the equivalent one-dimensional value. It is interesting to note that both the pressure and temperature rise generated by the fixed geometry REST inlet remain relatively constant between $M_1 = 3.6$ and 6.0. Furthermore, less than 16% of the mass flow compressed by the inlet spills below the cowl at $M_1 = 3.6$. Of the three Mach numbers examined, exit flow nonuniformity is greatest at $M_1 = 4.8$. Although the $M_1 = 3.6$ case is farthest from the design point, the greater wave angles associated with the lower Mach number flow produce considerable wave cancellation by the time flow reaches the exit plane.

Comparison with a Two-Dimensional Inlet

To gauge the effectiveness of the REST inlet, its performance can be compared with a classical two-dimensional inlet. Figure 10 shows a schematic of the two-dimensional, three-shock inlet configuration used for comparison. It is assumed to have shock angles optimized for maximum total pressure recovery, perfect shock reflection, an aspect ratio of $W/H = 4.0$, and the same normalized isolator length (L_{is}/d_h) as the REST inlet. Performance properties for the REST inlet are listed in Table 2. These may be directly compared with the performance properties of a two-dimensional inlet that generates the same pressure rise at the same entrance Mach number, listed in Table 3. The REST inlet has better performance than the two-dimensional inlet in terms of total pressure recovery, kinetic energy efficiency, and process efficiency even well below its design point. While the REST inlet has an L_{inl}/d_h similar to the $M_1 = 6.0$ two-dimensional inlet, the two-dimensional inlets used for comparison at $M_1 = 3.6$ and 4.8 are considerably shorter than the REST inlet. Despite this fact, the inviscid drag coefficient for the REST inlet is lower than the $M_1 = 4.8$ and 6.0 two-dimensional inlets, and is almost identical to the $M_1 = 3.6$ two-dimensional inlet. The values listed in Tables 2 and 3 constitute a satisfying result as an optimized two-dimensional, three-shock inlet is generally considered to have good performance. It is important to note, however, that the values listed in Tables 2 and 3 are only based on inviscid calculations and do not represent actual performance levels.

Table 1 Mach 6.0 REST inlet inviscid characteristics

Property	Mach 3.6	Mach 4.8	Mach 6.0
m_c	84.4%	94.0%	99.5%
P_R	$14.8 \pm 3.0\%$	$13.7 \pm 19.1\%$	$13.8 \pm 9.8\%$
T_R	$2.19 \pm 2.2\%$	$2.16 \pm 5.8\%$	$2.16 \pm 6.4\%$
M_{ex}	$1.77 \pm 2.7\%$	$2.82 \pm 5.3\%$	$3.74 \pm 4.2\%$

Table 2 REST inlet inviscid parameters

Property	Mach 3.6	Mach 4.8	Mach 6.0
P_T	0.960	0.932	0.926
η_{KE}	0.995	0.996	0.997
η_{KD}	0.990	0.982	0.981
C_D	0.349	0.185	0.114
L_{inl}/d_h	17.57	17.57	17.57

Table 3 Two-dimensional inlet inviscid parameters

Property	Mach 3.6	Mach 4.8	Mach 6.0
P_T	0.784	0.795	0.791
η_{KE}	0.972	0.985	0.990
η_{KD}	0.945	0.946	0.945
C_D	0.348	0.193	0.125
L_{inl}/d_h	7.90	13.26	18.08

Viscous Correction Calculations

General Remarks

The final stage of the design procedure involves calculation of a viscous correction to the inlet shape. Without enlargement of the

inlet to allow for boundary-layer growth, the overall pressure ratio generated during actual operation will be considerably higher than that predicted with the inviscid calculations. In the current work involving three-dimensionally curved inlets, the viscous correction must include some treatment of three-dimensional effects. However, full calculation of the corner flows at the entrance to the inlet or the shock-wave/boundary-layer interactions that occur throughout the inlet flowfield is not practical or desirable within a design procedure. In this instance, we simply wish to obtain a smooth correction to the inlet shape so that the actual inlet flowfield contains a core region that is similar to that predicted by the inviscid calculations. Therefore, the viscous correction performed in the current work neglects corner flows, smooths any abrupt changes in the boundary-layer displacement thickness caused by shock interactions, and makes use of the assumption that flow direction within the boundary layer does not vary greatly from the local inviscid flow direction. The corners are quickly smoothed out in a REST inlet, hence neglecting the corner flows should not degrade the accuracy of the viscous correction. Furthermore, smoothing the abrupt displacement thickness change that occurs at shock interactions is a necessity for the design of any practical hypersonic inlet. Finally, the assumption of small crossflow is considered to be reasonable for hypersonic REST inlets, except in the local region surrounding shock-wave interactions (with the usual caveat for large separations). As the details of the shock interaction region are smoothed out as part of the general viscous correction procedure, this deficiency should not be significant.

Small Crossflow Equations

Two useful concepts for the study of three-dimensional compressible boundary layers are streamline-based orthogonal coordinate systems and the analogy between the axisymmetric and small crossflow boundary-layer equations. A boundary layer on a curved surface can be represented by a streamline-based coordinate system in which the x-coordinate curves are formed by the projection of the inviscid streamlines onto the surface, the z-coordinate curves remain on the surface and are orthogonal to the x curves, and the y coordinate is normal to the surface. When using this system, the u-velocity component is called the *streamwise velocity* and the w-velocity component is called the *crossflow*. In general, flow in the boundary layer differs from the inviscid freestream by the crossflow angle $\beta = \tan^{-1}(w/u)$. In many high-speed flows where separation does not occur, β is small everywhere and the small crossflow assumptions may be used to simplify the full three-dimensional boundary-layer equations. In this instance, the continuity, streamwise momentum, and energy equations are decoupled from the crossflow momentum equation and are solved separately.[14] If the metrics of the x and z coordinates are represented by h_1 and h_2, these equations take the same form as the axisymmetric compressible boundary-layer equations with h_2 in place of the radius of the axisymmetric body and s as the distance along the streamline (where $\partial/\partial s = 1/h_1 \partial/\partial x$). These ideas are applicable to both laminar and turbulent flow. In solutions of the small crossflow equations, $\partial h_2/\partial s > 0$ indicates streamline divergence, $h_2 = \text{const}$ indicates parallel streamlines (i.e., locally two-dimensional flow), and $\partial h_2/\partial s < 0$ indicates streamline convergence. The inlet flowfields of interest in the current work include substantial variations in h_2; hence, use of a two-dimensional boundary-layer calculation would have resulted in a poor estimate of the inlet boundary layer.

Given the geometrical properties of the inviscid streamlines and a closure model for the turbulent terms, the small crossflow equations may be solved along each streamline using a finite difference boundary-layer code. The two-dimensional code described in Cebeci and Bradshaw[15] was adapted in the current work for use with nonisentropic edge conditions. This code uses the eddy-viscosity turbulence model from Cebeci and Smith.[16] Solution of the axisymmetric boundary-layer equations, or in this case, the small crossflow equations, was obtained by incorporating the Mangler transformation into the standard Levy–Lees transformation used in the code. In the unmodified code, the full-edge conditions are input at the starting station and the edge conditions in the remainder of the calculation are determined using the imposed pressure distribution and the assumption of isentropic flow. In the current work, the code was modified to read in both the pressure and velocity at the boundary-layer edge along the full length of the calculation. Furthermore, the standard substitution of $\rho_e u_e \partial u_e/\partial s$ for the $-\partial P_e/\partial s$ term in the streamwise momentum equation was bypassed. These necessary changes required some small additions to the standard code; however, its overall computational structure remained unchanged.

Viscous Correction to the Mach 6.0 REST Inlet

The viscous correction to the REST inlet was calculated at its design point with freestream conditions $M_1 = 6.02$, $P_1 = 2032$ Pa, and $T_1 = 63$ K, corresponding to $Re_1 = 2.6 \times 10^7$/m. An inlet capture width of 152 mm was chosen, boundary-layer transition was assumed to occur 12 mm downstream of leading edges, and an adiabatic wall assumption was made. Some results of the boundary-layer calculations performed for this viscous correction are described in the following paragraphs.

The inviscid calculations of the Mach 6.0 REST inlet flowfield were used to determine the paths of streamlines needed for boundary-layer calculations. Unfortunately, the tangency boundary condition used in GASPv3 causes an anomalous entropy layer to form at the wall downstream of shock/surface interactions. This defect is typical of upwind-biased CFD codes written specifically for solution of the Navier–Stokes equations. The extent of the flow area contaminated by this error can be minimized by grid clustering near walls, but can only be removed by using a more rigorous tangency boundary condition formulation. To mitigate the errors associated with the aforementioned numerical anomaly, significant grid clustering was employed near walls (see Fig. 7) and flow properties from the seventh node away from the wall were superimposed on adjacent wall nodes. Streamlines were then traced in the boundary surfaces of the inlet grid using the TECPLOT[9] stream-tracing routine.

Figure 11 shows the displacement thickness, skin friction coefficient, and imposed pressure distribution calculated along the streamline starting from the midpoint of the top leading edge of the inlet. The imposed pressure climbs steadily along the streamline until the throat region ($x \approx 0.7$ m), where it jumps quickly to a level approximately equal to that at the inlet exit. Boundary-layer displacement thickness grows quite quickly in the upstream section of the inlet, owed, in part, to the convergence of streamlines. Interestingly, this growth halts at the throat, dips slightly, then continues at a slow rate over the remaining inlet length. The sudden change in δ^* growth observed at the throat is a result of both the rapid pressure rise and cessation of streamline convergence that occurs in this region. The C_f distribution along this streamline is qualitatively similar to that which occurs on a constant pressure flat plate; however, it drops to an extremely low value at the exit of the inlet ($C_f \approx 0.0004$), as a consequence of the substantial streamline convergence that has occurred along its length. In general, streamline convergence leads to

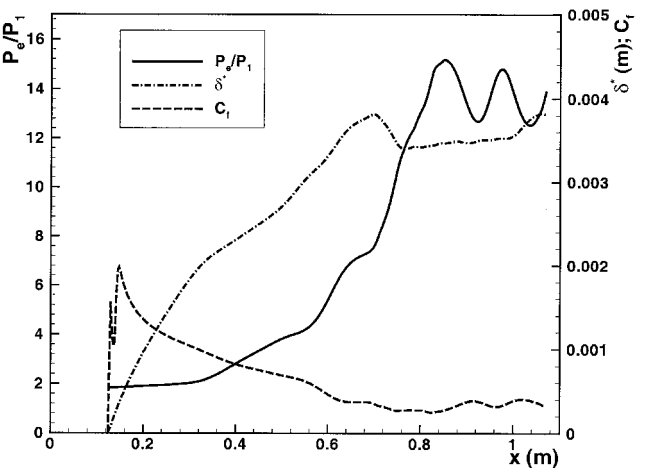

Fig. 11 Boundary-layer properties calculated along the streamline starting at the midpoint of the top leading edge of the REST inlet.

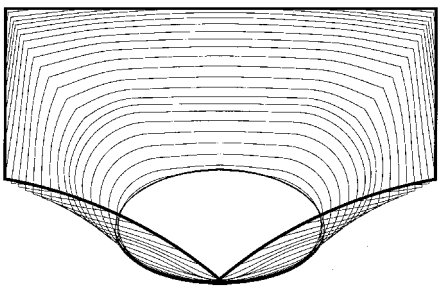

Fig. 12 Cross-sectional shape distribution for the viscous corrected Mach 6.0 REST inlet.

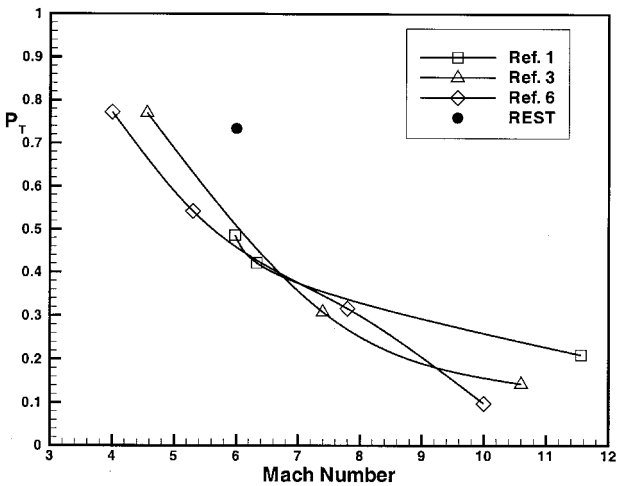

Fig. 13 Three-dimensional hypersonic inlet performance comparison.

a larger δ^* and a reduced C_f relative to a flat plate under the same pressure distribution. The boundary-layer parameter distributions shown in Fig. 11 are typical of those along most streamlines on the inlet surface.

Smoothed δ^* distributions calculated along 36 streamlines starting at the leading edges of each of the top, side, and bottom surfaces were added to the inviscid shape of the inlet, thereby increasing its cross-sectional area. The cross sections of the viscous corrected inlet shape are shown in Fig. 12. No boundary-layer calculations were instigated at the inlet corners, so that the coordinates corresponding to the corners of each cross section were calculated by extrapolation from adjacent points. Only subtle differences between the inviscid and viscous corrected shapes are apparent (compare Fig. 12 with Fig. 3); however, the overall contraction ratio of the inlet has reduced to $CRT_{\text{vis}} = 4.67$, with an internal contraction ratio of $CRI_{\text{vis}} = 2.12$. While a $CRI = 2.12$ is greater than the Kantrowitz starting limit, experimental results of Refs. 1–3 suggest that inlets of this class can self-start at Mach 6 with significantly higher CRI than indicated by this one-dimensional inviscid limit. The actual starting characteristics of the REST inlet down to ramjet takeover speeds will need to be determined by experiment.

With the completion of the viscous correction, a more realistic estimate of the inlet performance parameters may be made. The flow exiting the inlet consists of approximately 36% boundary layer by mass. Equivalent one-dimensional stream thrust conserved performance parameters obtained by combining the boundary layer and core flows of the REST inlet are listed in Table 4, along with the corresponding inviscid values. While the estimated performance of the actual inlet is significantly reduced from its inviscid level, these values correspond to those of an efficient scramjet inlet at Mach 6.0. Figure 13 shows a comparison of the REST inlet with three-dimensional inlet test data reported in Refs. 1, 3, and 6 in terms of mass flow weighted total pressure recovery, $(P_T)_{\text{mfw}}$. While comparison of inlets with different compression ratios, mass captures, and design Mach numbers is somewhat arbitrary, Fig. 13 does indicate that REST inlets designed using the current procedure promise

Table 4 Comparison of REST inlet inviscid and viscous parameters at Mach 6.0

Parameter	Inviscid	Viscous
P_R	13.78	13.54
T_R	2.16	2.60
M_{ex}	3.74	3.28
P_T	0.926	0.465
η_{KE}	0.997	0.966
η_{KD}	0.981	0.849

better inlet efficiency than similar fixed geometry configurations designed and tested in the 1960s. The superior performance of the REST inlet is believed to be a result of both the inclusion of the three-dimensional boundary-layer correction in the design procedure, and to the optimization of the inlet shape transition. Neither of these steps were included in the design of the inlets described in Refs. 1–3 and 6. The marked difference between $(P_T)_{\text{mfw}} = 0.734$ and the stream thrust conserved value of $P_T = 0.465$ shown in Table 4 highlights the importance of using consistent calculation methods when comparing hypersonic inlet performance.

Conclusions

A methodology was presented for the design of three-dimensional hypersonic inlets with rectangular-to-elliptical shape transition. These fixed geometry inlets included highly swept leading edges and a significantly notched cowl to allow the possibility of self-starting at ramjet take-over speeds. The inviscid portion of the design procedure made extensive use of streamtracing methods and a mathematical lofting technique to determine an aerodynamically efficient shape transition. Furthermore, the surface pressure signature of the inlet flowfield was compared with established correlations to check for shock-induced boundary-layer separation. The final step in the procedure involved a simplified three-dimensional turbulent boundary-layer calculation for determination of the physical inlet shape that generates the desired inviscid flowfield. This design procedure utilized currently available computational tools and high-speed computers to perform the numerous cycles needed to complete a design.

The characteristics of a Mach 6.0 inlet designed with the current methodology were described. Inviscid flowfield calculations indicated that this inlet exhibited good on-design performance while generating a relatively uniform exit flow and low drag coefficient. This was considered to be a significant achievement given its substantial shape transition. Examination of the off-design inviscid performance down to Mach 3.6 indicated an increased level of exit flow nonuniformity and a minimum mass capture of 84.4%. However, its performance remained above that of a two-dimensional inlet optimized for maximum total pressure recovery. Completion of the viscous correction allowed equivalent one-dimensional stream thrust conserved performance estimates of $P_T = 0.465$, $\eta_{KE} = 0.966$, and $\eta_{KD} = 0.849$ to be obtained for the actual inlet. If realized in practice, these levels correspond to an efficient inlet for scramjet applications. This work clearly shows the performance advantages that may be gained through the use of three-dimensional inlet geometries relative to more traditional inlet configurations designed using two-dimensional techniques.

Acknowledgments

The author would like to thank G. Anderson, C. Trexler, and A. Auslender for many useful discussions, and K. Tatum for assistance with the computations. This research has been supported by the National Research Council, Research Associate Program and the Hypersonic Airbreathing Propulsion Branch at NASA Langley Research Center.

References

[1] Hartill, W. B., "Analytical and Experimental Investigation of a Scramjet Inlet of Quadriform Shape," U.S. Air Force, TR AFAPL-TR-65-74, Marquardt Corp., Aug. 1965.

[2]Kiersey, J. L., and Snow, M. L., "Modular Inlet Investigation," Aeronautics Div., Research and Development, Applied Physics Lab., Quarterly Rept. AQR/66-1, Johns Hopkins Univ., Baltimore, MD, Jan. 1966.

[3]Kutshenreuter, P. H., "Hypersonic Inlet Tests in Helium and Air," AIAA Propulsion Joint Specialist Conf., U.S. Air Force Academy, CO, June 1965.

[4]Kantrowitz, A., and Donaldson, C., "Preliminary Investigation of Supersonic Diffusers," NACA ACR L5D20, May 1945.

[5]Simmons, J. M., and Weidner, E. H., "Design of Scramjet Inlets with Rectangular to Circular Shape Transition," NASA TM 87752, June 1986.

[6]Billig, F. S., "Supersonic Combustion Ramjet Missile," *Journal of Propulsion and Power*, Vol. 11, No. 6, 1995, pp. 1139–1146.

[7]Smart, M. K., "Calculation of Streamtraced Hypersonic Inlet Performance On and Off Design," 21st International Symposium on Shock Waves, Paper 5330, Great Keppel, Australia, July 1997.

[8]Salas, M. D., "Shock Fitted Method for Complicated Two-Dimensional Supersonic Flows," *AIAA Journal*, Vol. 14, No. 5, 1976, pp. 583–588.

[9]*Amtec Engineering TECPLOT™ Version 6 Users Manual*, Amtec Engineering, Inc., Bellevue, WA, 1993.

[10]Barger, R. L., "A Procedure for Designing Forebodies with Constraints on Cross-Section Shape and Axial Area Distribution," NASA TP 1881, July 1981.

[11]Korkegi, R. H., "Comparison of Shock Induced Two- and Three-Dimensional Incipient Turbulent Separation," *AIAA Journal*, Vol. 13, No. 4, 1975, pp. 534, 535.

[12]Korkegi, R. H., "A Lower Bound for Three-Dimensional Turbulent Separation in Supersonic Flow," *AIAA Journal*, Vol. 23, No. 3, 1985, pp. 475, 476.

[13]*Aerosoft Inc. GASP Version 3 Users Manual*, Aerosoft, Inc., Blacksburg, VA, 1996.

[14]Cooke, J. C., "Axially Symmetric Analogue for General Three-Dimensional Boundary Layers," Aeronautical Research Council, RM 3200, June 1959.

[15]Cebeci, T., and Bradshaw, P., *Physical and Computational Aspects of Convective Heat Transfer*, Springer–Verlag, New York, 1994.

[16]Cebeci, T., and Smith, A. M. O., *Analysis of Turbulent Boundary Layers*, Academic, New York, 1974.